ISSN 1063-7737, Astronomy Letters, 2012, Vol. 38, No. 2, pp. 101–116. © Pleiades Publishing, Inc., 2012.
Original Russian Text © Yu.V. Pakhomov, 2012, published in Pis'ma v Astronomicheskiĭ Zhurnal, 2012, Vol. 38, No. 2, pp. 122–137.

Chemical Composition of the Atmospheres of Red Giants with High Space Velocities

Yu. V. Pakhomov*

Institute of Astronomy, Russian Academy of Sciences, Pyatnitskaya ul. 48, Moscow, 109017 Russia

Received September 27, 2011

Abstract—The results of a comparative analysis of the elemental abundances in the atmospheres of 14 red giants with high Galactic space velocities are presented. For almost all of the chemical elements considered, the their abundance trends with metallicity correspond to those constructed for thick-disk dwarfs. In the case of sodium, the main factor affecting the [Na/Fe] abundance in the stellar atmosphere for red giants is the surface gravity that characterizes the degree of development of the convective envelope. The difference between the [Na/Fe] abundances in the atmospheres of thin- and thick-disk red giants has been confirmed.

DOI: 10.1134/S1063773712020053

Keywords: *stellar spectroscopy, stellar atmospheres, red giants, stellar evolution, kinematics, Galactic chemical evolution.*

INTRODUCTION

Our Galaxy is currently believed to be a set of subsystems that differ by their sizes, locations in the Galaxy, characteristic stellar velocities, and stellar populations. The best-known subsystems are the nucleus, the bulge, the thick and thin disks, and the halo. Each subsystem can contain dynamical stellar groups or streams (see, e.g., Eggen 1958a, 1958b). At a Galactocentric distance of about 8.5 kpc, where the Solar system is located, there are stars of at least three Galactic subsystems: the thick and thin disks and the halo. In addition, stars with significant orbital eccentricities that can belong to the bulge exist in the inner Galaxy. Such stars are characterized by an enhanced metallicity, and super-metal-rich stars are more often observed among the bulge objects (Pakhomov et al. 2009b). In contrast, the halo stars exhibit a low metallicity and a large scatter of orbital inclinations and eccentricities. Thus, the structure and chemical evolution of the Galaxy can be investigated by studying the motion of stars in the solar neighborhood, their physical characteristics, and the abundances of chemical elements in their atmospheres.

The chemical composition of the stellar atmospheres changes as the star on the temperature–luminosity diagram passes from the main sequence to the red giant branch in the course of its evolution. The hydrogen burning reactions cease in the core and begin in the shell around the core. At this stage of its life, the structure of the star changes significantly: the star rapidly expands, and an extensive convective shell that provides the first deep mixing of stellar matter is formed. The nuclear burning products are brought into the stellar atmosphere and become observable. The changes in the CNO abundances are well known: carbon and oxygen are reduced approximately by 0.1–0.3 dex, while nitrogen is enhanced by 0.1–0.4 dex. In addition to these elements, the changes can also affect other elements.

In this paper, we analyze the chemical composition of red giants with Galactic velocities that exceed those typical of thin-disk stars in the solar neighborhood and the main causes of the changes in elemental abundances. These changes reflect not only the chemical evolution of the Galactic subsystem to which they belong but also the stellar evolution processes.

OBSERVATIONS

We selected the stars for our observations based on their Galactic velocities calculated from reduced Hipparcos parallaxes (van Leeuwen 2007) and CORAVEL radial velocities (Maurice et al. 1987). We chose the red giants for which at least one of the Galactic velocity vector components (UVW) exceeded its typical values for the thin disk (34.5, 22.5, 18.0) km s^{-1} (Famaey et al. 2005). The effective temperatures $T_{\rm eff}$ and surface gravities $\log g$ for the program stars were preestimated from photometric data and reduced Hipparcos parallaxes

*E-mail: pakhomov@inasan.ru

Table 1. The list of investigated stars with the membership probabilities (p) in some Galactic subsystems

No.	HD	α_{2000}	δ_{2000}	m_V	Spectral type	p, %		
						thin disk	Hercules stream	thick disk
1	2901	$00^h32^m47^s.6$	+54°07′11″	6.91	K2III	–	–	99
2	10550	01 42 43.5	−03 41 24	4.98	K3II-III	27	58	13
3	92095	10 39 05.7	+53 40 05	5.55	K3III	16	–	83
4	94600	10 55 44.4	+33 30 25	5.02	K1III	91	–	8
5	94669	10 56 14.5	+42 00 29	6.03	K2III	30	41	27
6	94860	10 59 56.8	+77 46 12	6.18	G9III	15	4	80
7	99902	11 29 41.9	+15 24 47	5.74	K4III	87	–	11
8	100696	11 36 02.7	+69 19 22	5.19	K0III	52	–	47
9	104985	12 05 15.1	+76 54 20	5.78	G9III	38	–	61
10	127243	14 28 37.8	+49 50 41	5.58	G3IV	–	–	99
11	141353	15 48 13.3	+13 47 21	5.98	K2III	1	1	97
12	141472	15 46 34.7	+55 28 29	5.94	K3III	–	–	99
13	152879	16 55 22.2	+18 25 59	5.35	K4III	4	–	95
14	197752	20 44 52.5	+25 16 14	4.92	K2III	41	–	58

(van Leeuwen 2007). Subsequently, the stars with effective temperatures $T_{\rm eff}$ from 4000 to 5200 K and surface gravities log$g$ from 0.5 to 3.0 were chosen from the list. The list of program stars is presented in Table 1.

The spectroscopic observations of the chosen stars were performed in 2007–2008 with a two-band echelle spectrograph attached to a 2.16-m telescope at the Xinglong station of the National Astronomical Observatories of China (NAOC). The spectrograph operated in the red-band mode. The detector was a 1024×1024 CCD array on which 40 spectral orders in the range from 5565 to 9194 Å were recorded. The spectrograph resolution was $R = 40\,000$; the signal-to-noise ratio in the spectra was $S/N > 150$.

The *echelle* package of the *MIDAS* software system was used for the spectroscopic data reduction, the search for and extraction of the spectral orders, the wavelength calibration using the spectrum of a thorium–argon lamp, and the spectrum normalization. The equivalent widths of the selected spectral lines were measured in the *EW* code that I wrote.

DETERMINING THE PARAMETERS OF THE STELLAR ATMOSPHERES

Table 2 gives the parameters of the stellar atmospheres (effective temperature $T_{\rm eff}$, surface gravity log g, microturbulence V_t, and metallicity [Fe/H]), the stellar masses and ages on a logarithmic scale, and the interstellar extinctions A_V. We determined the masses and ages based on the evolutionary tracks from Girardi et al. (2000) by taking into account the stellar metallicity. The interstellar extinctions were estimated from the color excesses E($B-V$), E($V-J$), E($V-H$), E($V-K$), E($b-y$); the normal colors were calculated from the calibrations by Bessell et al. (1998), which are based on Kurucz's model

Table 2. Atmospheric parameters of the investigated stars, their physical parameters, and interstellar extinctions

No.	HD	$T_{\rm eff}$, K	$\log g$	V_t, km s^{-1}	[Fe/H]	Mass, $M_\odot$	Age log, yr	A_V
1	2901	4350	2.15	1.25	−0.46	0.7 ± 0.3	9.4 ± 0.5	$0^m.1$
2	10550	4290	1.25	1.50	0.05	7 ± 1	7.7 ± 0.4	0.1
3	92095	4430	2.15	1.38	−0.02	1.9 ± 0.3	9.0 ± 0.3	<0.1
4	94600	4660	2.50	1.20	−0.05	1.7 ± 0.3	9.0 ± 0.3	0
5	94669	4620	2.65	1.25	0.00	1.5 ± 0.4	8.9 ± 0.2	0
6	94860	4970	2.75	1.20	−0.03	2.8 ± 0.3	8.7 ± 0.2	<0.1
7	99902	4380	2.25	1.30	0.22	1.9 ± 0.5	9.0 ± 0.3	<0.1
8	100696	4920	2.70	1.26	−0.21	2.4 ± 0.3	8.6 ± 0.3	0
9	104985	4830	2.80	1.28	−0.10	1.9 ± 0.3	9.0 ± 0.3	0
10	127243	5100	1.75	1.28	−0.44	1.6 ± 0.3	9.1 ± 0.3	0
11	141353	4280	1.95	1.37	−0.09	2.0 ± 0.4	9.0 ± 0.4	<0.1
12	141472	4180	1.50	1.40	−0.27	1.1 ± 0.3	9.0 ± 0.5	<0.1
13	152879	4170	1.80	1.39	0.02	1.4 ± 0.5	9.5 ± 0.5	<0.1
14	197752	4570	2.25	1.33	0.03	2.6 ± 0.5	8.8 ± 0.5	<0.1

stellar atmospheres (Castelli and Kurucz 2003). We determined the parameters of the stellar atmospheres using a technique that is also based on Kurucz's model atmospheres (Castelli and Kurucz 2003) and analysis of the relative abundances of iron-peak elements. The technique is described in detail in Boyarchuk et al. (2001) and allows the parameters of the stellar atmospheres for G–K giants to be determined with an accuracy of about 70–100 K for $T_{\rm eff}$, 0.10–0.15 for $\log g$, and 0.10–0.15 km s^{-1} for V_t. In this paper, when analyzing the relative abundances of iron-peak elements when determining the parameters of the stellar atmospheres, we disregarded titanium, because it is well known that the [Ti/Fe] abundance can be enhanced at low metallicities and for thick-disk stars (Bensby et al. 2005). Using the derived parameters, we computed the corresponding model stellar atmospheres with the ATLAS9 code (Kurucz 1993). Based on the measured equivalent widths of the selected unblended spectral lines, we estimated the elemental abundances with the WIDTH9 code. These are presented in Table 3 and Fig. 1, where the open circles and asterisks denote the abundances determined from the spectral lines of neutral and ionized atoms, respectively. The list of selected lines with their characteristics and equivalent widths is available in electronic form. The cobalt abundance was determined by taking into account the hyperfine splitting effect, which can be strong in the case of cool giants (Boyarchuk et al. 2008). The abundance errors given in Table 3 and marked by the bars in Fig. 1 were determined as the dispersion of the individual abundances calculated from individual spectral lines. The possible abundance errors associated with the determination of stellar atmosphere parameters are listed in Table 4 for the stars HD 100673 ($T_{\rm eff} = 4920$ K, $\log g = 2.70$, $V_t = 1.26$ km s^{-1}) and HD 152879 ($T_{\rm eff} = 4170$ K, $\log g = 1.80$, $V_t = 1.39$ km s^{-1}) as an example. Table 4 gives the number of lines used (N) and the changes in the abundance of each element when changing individual model parameters ($\Delta T_{\rm eff} = +100$ K, $\Delta \log g =$

Table 3. Elemental abundances in the atmospheres of the program stars

Parameter	HD 2901		HD 10550		HD 92095		HD 94600		HD 94669		HD 94860		HD 99902	
	N	[El/H]	N	[El/H]	N	[El/H]	N	[El/H]	N	[El/H]	N	[El/H]	N	[El/H]
Na I	2	-0.39 ± 0.04	2	0.67 ± 0.08	2	-0.04 ± 0.04	2	-0.04 ± 0.07	2	0.00 ± 0.04	2	0.27 ± 0.02	2	0.40 ± 0.04
Mg I	2	-0.12 ± 0.01	2	0.16 ± 0.02	2	0.06 ± 0.02	2	0.00 ± 0.00	2	0.04 ± 0.01	2	0.24 ± 0.02	2	0.30 ± 0.08
Al I	2	-0.12 ± 0.04	2	0.21 ± 0.07	2	0.04 ± 0.03	2	-0.05 ± 0.00	2	0.16 ± 0.08	2	0.26 ± 0.01	2	0.32 ± 0.05
Si I	8	-0.18 ± 0.07	2	0.04 ± 0.01	7	0.06 ± 0.06	10	-0.02 ± 0.07	9	0.06 ± 0.08	8	0.10 ± 0.03	8	0.29 ± 0.08
Ca I	3	-0.22 ± 0.07	–		3	0.02 ± 0.07	4	0.11 ± 0.12	3	0.13 ± 0.06	4	0.13 ± 0.02	3	0.29 ± 0.06
Sc I	–	–	–	–	1	0.03	2	-0.04 ± 0.14	2	0.24 ± 0.14	1	0.30	–	–
Sc II	5	-0.12 ± 0.06	2	0.06 ± 0.03	4	0.18 ± 0.05	3	0.00 ± 0.03	5	0.15 ± 0.06	3	0.39 ± 0.03	4	0.28 ± 0.10
Ti I	20	-0.18 ± 0.07	5	0.01 ± 0.03	20	-0.05 ± 0.06	25	-0.07 ± 0.06	24	0.01 ± 0.08	24	0.18 ± 0.05	14	0.24 ± 0.06
V I	7	-0.13 ± 0.07	2	-0.04 ± 0.01	7	0.10 ± 0.08	20	0.00 ± 0.06	13	0.15 ± 0.07	25	0.18 ± 0.07	3	0.21 ± 0.07
Cr I	6	-0.46 ± 0.07	4	-0.03 ± 0.08	7	-0.11 ± 0.09	11	-0.10 ± 0.09	10	0.00 ± 0.07	9	-0.05 ± 0.05	8	0.15 ± 0.09
Mn I	1	-0.79	1	-0.17	1	-0.29	1	-0.31	1	-0.19	–	–	1	0.03
Fe I	66	-0.46 ± 0.06	16	0.05 ± 0.07	58	-0.02 ± 0.06	73	-0.05 ± 0.06	63	0.00 ± 0.07	66	-0.03 ± 0.06	55	0.22 ± 0.07
Fe II	6	-0.48 ± 0.10	4	0.00 ± 0.07	6	-0.07 ± 0.10	5	-0.07 ± 0.08	5	0.00 ± 0.06	5	-0.07 ± 0.07	2	0.13 ± 0.03
Co I	4	-0.40 ± 0.08	4	0.05 ± 0.09	4	0.04 ± 0.08	5	-0.11 ± 0.07	5	0.04 ± 0.07	5	0.07 ± 0.12	8	0.27 ± 0.09
Ni I	21	-0.40 ± 0.06	6	0.01 ± 0.05	13	-0.03 ± 0.06	18	-0.09 ± 0.05	14	0.03 ± 0.07	18	0.03 ± 0.07	14	0.23 ± 0.06
Y II	–	–	–	–	–	–	–	–	–	–	1	-0.32	2	0.14 ± 0.03
Zr II	–	–	1	-0.06	1	0.09	1	0.23	1	0.23	–	–	1	0.18
Mo I	2	-0.42 ± 0.02	–	–	1	-0.31	–	–	–	–	1	-0.02	1	0.06
Ba II	1	-0.15	–	–	1	0.56	1	0.15	1	0.53	1	0.06	–	–
La II	–	–	1	0.07	–	–	–	–	–	–	–	–	1	0.15
Ce II	1	-0.45	–	–	1	0.79	1	0.37	1	0.83	1	0.24	1	0.39
Nd II	4	-0.29 ± 0.06	1	0.07	3	0.22 ± 0.06	2	0.17 ± 0.10	1	-0.03	–	–	2	0.42 ± 0.02
Eu II	1	0.03	1	0.13	1	0.10	1	0.06	1	0.15	1	0.28	1	0.37

Table 3. (Contd.)

Parameter	HD 100696		HD 104985		HD 127243		HD 141353		HD 141472		HD 152879		HD 197752	
	N	[El/H]	N	[El/H]	N	[El/H]	N	[El/H]	N	[El/H]	N	[El/H]	N	[El/H]
Na I	2	-0.21 ± 0.03	2	-0.10 ± 0.02	3	-0.58 ± 0.03	2	-0.03 ± 0.03	2	-0.31 ± 0.02	2	0.28 ± 0.07	2	0.17 ± 0.04
Mg I	2	-0.10 ± 0.02	2	0.11 ± 0.00	2	-0.15 ± 0.03	2	0.18 ± 0.01	2	-0.03 ± 0.01	2	0.20 ± 0.09	2	0.15 ± 0.03
Al I	2	-0.12 ± 0.01	2	0.12 ± 0.05	2	-0.26 ± 0.02	2	0.10 ± 0.09	2	-0.03 ± 0.12	1	-0.02	2	0.12 ± 0.08
Si I	10	-0.10 ± 0.08	13	0.08 ± 0.05	10	-0.29 ± 0.07	8	0.13 ± 0.07	8	-0.13 ± 0.06	7	0.13 ± 0.09	6	0.05 ± 0.04
Ca I	4	-0.04 ± 0.04	3	0.06 ± 0.04	4	-0.25 ± 0.05	3	-0.04 ± 0.07	4	-0.17 ± 0.05	2	0.06 ± 0.00	3	0.13 ± 0.05
Sc I	2	-0.17 ± 0.11	1	0.15	1	-0.67	–	–	1	-0.14	–	–	1	0.05
Sc II	4	-0.14 ± 0.07	5	0.25 ± 0.07	3	-0.37 ± 0.07	5	-0.02 ± 0.09	5	-0.08 ± 0.07	3	0.02 ± 0.11	6	0.08 ± 0.04
Ti I	24	-0.19 ± 0.06	20	0.03 ± 0.07	15	-0.27 ± 0.07	17	-0.07 ± 0.08	13	-0.15 ± 0.05	9	0.02 ± 0.08	20	0.00 ± 0.06
V I	26	-0.20 ± 0.08	18	0.07 ± 0.07	8	-0.44 ± 0.02	3	-0.16 ± 0.05	3	-0.11 ± 0.04	1	0.30	6	0.15 ± 0.05
Cr I	8	-0.21 ± 0.08	7	-0.13 ± 0.05	1	-0.56	11	-0.19 ± 0.11	4	-0.31 ± 0.04	6	0.00 ± 0.07	11	-0.02 ± 0.04
Mn I	1	-0.38	1	-0.53	1	-0.84	1	-0.36	1	-0.81	–	–	1	-0.20
Fe I	79	-0.21 ± 0.06	69	-0.10 ± 0.06	53	-0.51 ± 0.08	57	-0.09 ± 0.07	51	-0.33 ± 0.08	38	0.02 ± 0.05	62	0.03 ± 0.05
Fe II	6	-0.20 ± 0.08	5	-0.12 ± 0.08	6	-0.57 ± 0.07	4	-0.11 ± 0.07	3	-0.44 ± 0.09	2	0.00 ± 0.11	4	0.01 ± 0.04
Co I	4	-0.27 ± 0.05	5	-0.02 ± 0.07	2	-0.39 ± 0.00	6	0.10 ± 0.05	6	-0.26 ± 0.07	4	0.12 ± 0.07	5	-0.04 ± 0.08
Ni I	25	-0.22 ± 0.07	20	-0.06 ± 0.05	13	-0.50 ± 0.07	11	-0.07 ± 0.05	9	-0.30 ± 0.05	6	-0.03 ± 0.07	15	0.03 ± 0.06
Y II	1	-0.15	–	–	–	–	1	-0.25	2	-0.21 ± 0.02	1	1.20	1	-0.02
Zr II	1	0.03	–	–	–	–	1	-0.09	1	-0.06	–	–	1	-0.06
Ba II	1	0.09	1	0.14	1	-0.36	1	0.14	–	–	–	–	1	0.29
Ce II	–	–	–	–	–	–	–	–	1	0.16	–	–	1	0.47
Nd II	2	0.10 ± 0.14	1	0.04	–	–	2	0.01 ± 0.10	3	0.03 ± 0.09	2	0.09 ± 0.10	2	0.10 ± 0.06
Eu II	1	-0.08	1	0.20	1	-0.31	1	0.09	1	-0.03	1	0.09	1	0.12

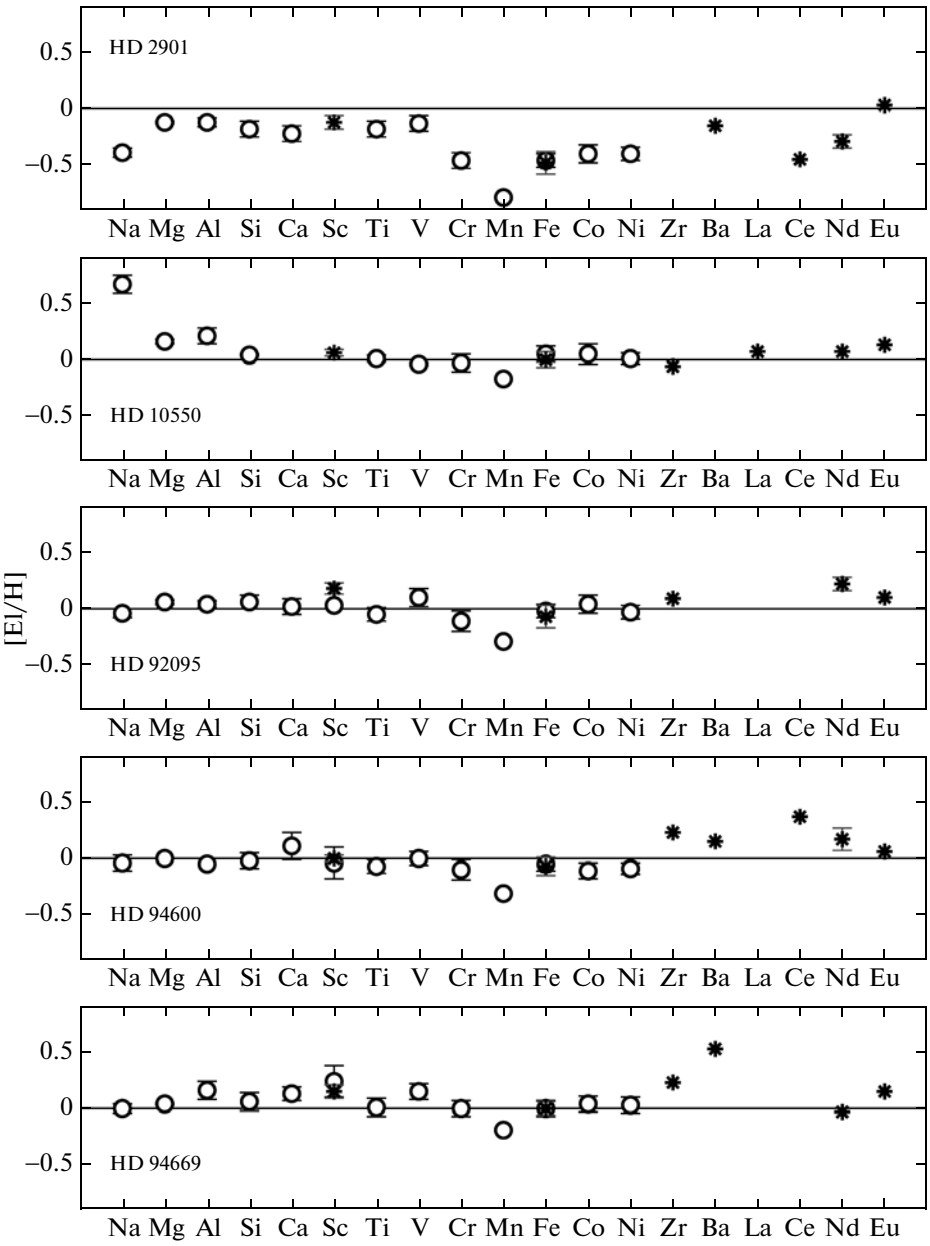

Fig. 1. Relative elemental abundances in the atmospheres of the program stars. The open circles and asterisks denote the abundances determined from spectral lines of neutral and ionized atoms, respectively.

$+0.10$, $\Delta V_t = +0.10$ km s^{-1}) and the total change in abundance Δ.

STELLAR KINEMATICS

The last columns in Table 1 give the membership probabilities of the program stars in Galactic subsystems whose kinematic characteristics were taken from Famaey et al. (2005). We calculated the probabilities based on the formulas from Mishenina et al. (2004). Table 1 includes the thick and thin disks and the Hercules stellar stream, because it turned out that some of the stars could also belong to the latter. In our previous paper (Pakhomov et al. 2011) devoted to the Hercules stellar stream, we showed that the stream is inhomogeneous in its composition and could contain both thin- and thick-disk stars. The membership probability in the halo and other subsystems and moving stellar groups are not given in Table 1, because it turned out to be less than 1% for all program stars.

Table 5 presents the kinematic characteristics of

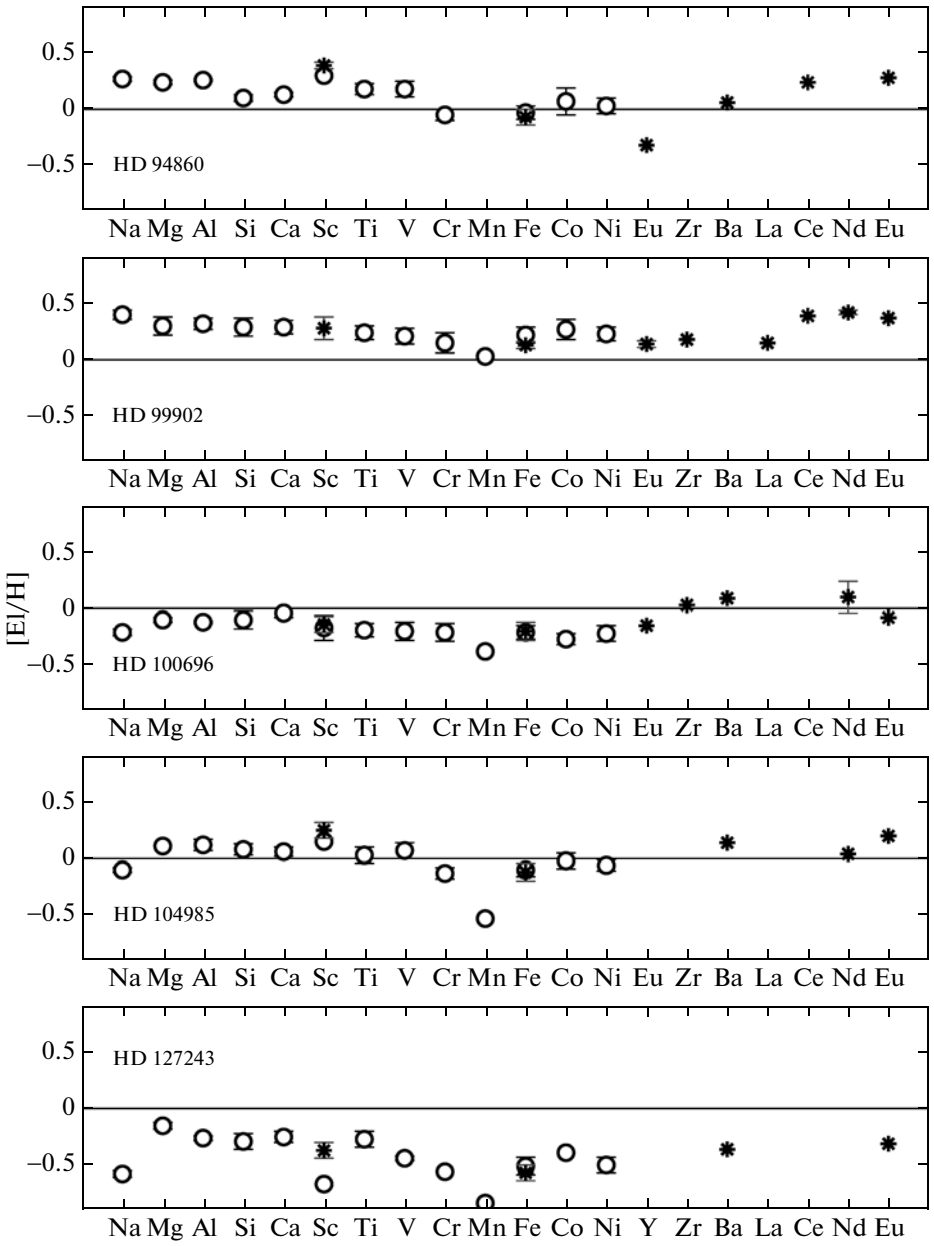

Fig. 1. (Contd.)

the program stars. These include the Galactic velocity vector (U, V, W) relative to the Sun and the Galactic orbital elements: the perigalactic distance $R_{\min}$, the apogalactic distance $R_{\max}$, the maximum orbital distance from the Galactic plane $Z_{\max}$, the eccentricity e, and the inclination i. The distance to the Galactic center was assumed to be 8.5 kpc, while the necessary correction of the velocities for the solar motion, (+10.2, +14.9, +7.8) km s^{-1}, was taken from Famaey et al. (2005). We calculated the orbital elements through numerical integration of the stellar motion by Everhart's 15th-order method using a three-component model Galactic potential (Allen and Santillan 1991). The integration accuracy was controlled by the conservation of the necessary integrals of motion. For example, in ten orbital revolutions, the typical relative error was $\Delta h/h < 10^{-13}$ in angular momentum and $\Delta E/E < 10^{-8}$ in total energy. The errors in the space velocities (σU, σV, σW) were calculated from the errors in the stellar proper motions, radial velocities, parallaxes and the errors in the solar velocity components relative to the local standard of rest. We calculated the errors in the Galactic orbital elements based on the model Galactic gravitational

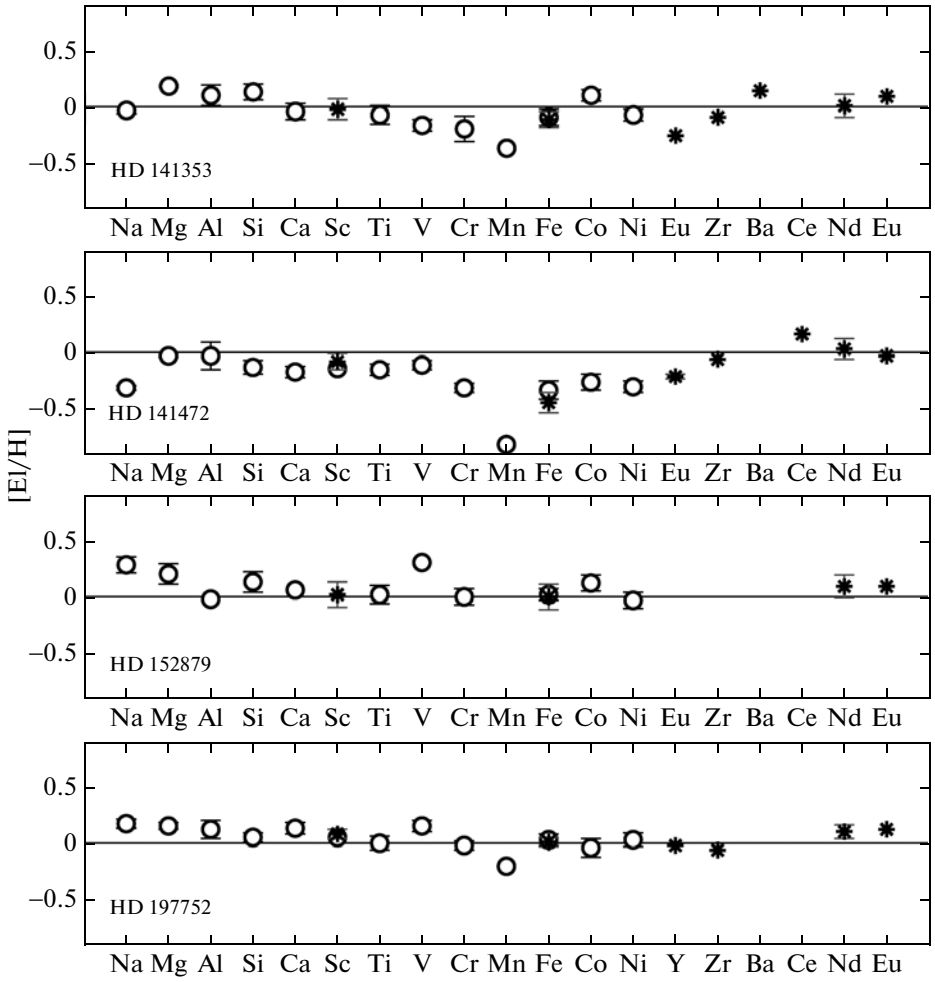

Fig. 1. (Contd.)

potential using the probable errors in the stellar space velocities.

We see from Table 1 that the membership probability in the thin disk at least for two stars (HD 94600 and HD 99902) exceeds considerably that for the thick disk and these probabilities are almost equal for one star (HD 100696). However, these stars were also included in our program, because the maximum orbital distance from the Galactic plane $Z_{\max}$ for them exceeds the characteristic scale height for thin-disk objects, 90–325 pc (Gilmore and Reid 1983; Robin et al. 1996; Chen et al. 2001).

DISCUSSION

Figure 2 presents the [Na/Fe], [Mg/Fe], [Al/Fe], [Si/Fe], [Ca/Fe], and [Ti/Fe] abundance trends with metallicity in the atmospheres of the red giants investigated here (the large circles with ordinal numbers from Table 1) in comparison with other stars. The small filled circles indicate the 74 thin-disk red giants from Antipova and Boyarchuk (2001), Boyarchuk et al. (2002, 2008), Antipova et al. (2003, 2004, 2005), and Pakhomov et al. (2009a, 2009b, 2011) that we investigated by a unified technique. The filled and open triangles indicate the thin-disk (29 stars) and thick-disk (22 stars) red giants from Alves-Brito et al. (2010), which is devoted to the investigation of the Galactic chemical evolution in the solar neighborhood. The solid and dashed lines indicate the thin- and thick-disk dwarfs from Bensby et al. (2005) averaged with a metallicity interval of 0.2 dex, while the shaded regions denote a dispersion of 1σ.

The six chemical elements in Fig. 2 are among the indicators of the Galactic chemical evolution, with four of them being represented by the α-elements Mg, Si, Ca, and Ti. We see from Fig. 2 that the behavior of all elements, except sodium, in the atmospheres of the red giants is similar to that for the dwarfs.

Table 4. Changes of the elemental abundances in the atmospheres of the stars HD 100673 ($T_{\rm eff} = 4920$ K, $\log g = 2.70$, $V_t = 1.26$ km s^{-1}) and HD 152879 ($T_{\rm eff} = 4170$ K, $\log g = 1.80$, $V_t = 1.39$ km s^{-1}) when changing the model parameters by $\Delta T_{\rm eff} = +100$ K, $\Delta \log g = +0.10$, $\Delta V_t = +0.10$ km s^{-1} and the total change in abundance Δ

Element	N	Δ[El/H]$_{\rm HD\ 100673}$				N	Δ[El/H]$_{\rm HD\ 152879}$			
		$\Delta T_{\rm eff}$	$\Delta \log g$	ΔV_t	Δ		$\Delta T_{\rm eff}$	$\Delta \log g$	ΔV_t	Δ
NA1	2	0.07	0.00	−0.02	0.07	2	0.07	−0.01	−0.05	0.09
MG1	2	0.05	0.00	−0.01	0.05	2	−0.03	0.01	−0.03	0.04
AL1	2	0.05	0.00	−0.01	0.05	1	0.06	0.00	−0.03	0.07
SI1	10	−0.02	0.01	−0.02	0.03	7	−0.10	0.03	−0.02	0.11
CA1	4	0.10	0.00	−0.04	0.11	2	0.11	0.00	−0.04	0.12
SC1	2	0.14	0.00	−0.01	0.14					
SC2	4	−0.01	0.05	−0.02	0.05	3	−0.03	0.04	−0.03	0.06
TI1	24	0.12	−0.01	−0.02	0.12	9	0.11	0.00	−0.04	0.12
V1	26	0.15	0.00	−0.02	0.15	1	0.13	0.01	−0.04	0.14
CR1	8	0.09	0.00	−0.01	0.09	6	0.09	0.01	−0.03	0.10
MN1	1	0.07	0.00	0.00	0.07					
FE1	79	0.07	0.01	−0.02	0.07	38	−0.02	0.03	−0.03	0.05
FE2	6	−0.08	0.05	−0.04	0.10	2	−0.22	0.07	−0.04	0.23
CO1	4	0.09	0.02	0.00	0.09	4	0.00	0.03	−0.02	0.04
NI1	25	0.05	0.01	−0.03	0.06	6	−0.04	0.03	−0.04	0.06
Y2	1	−0.01	0.05	0.00	0.05	1	−0.03	0.03	−0.03	0.05
ZR2	1	−0.01	0.05	0.00	0.05					
BA2	1	0.02	0.03	−0.11	0.12					
ND2	2	0.01	0.05	0.00	0.05	2	0.01	0.03	−0.02	0.04
EU2	1	−0.01	0.05	−0.01	0.05	1	−0.01	0.04	−0.02	0.05

Table 5. Kinematic parameters of the investigated stars

No.	HD	U, km s^{-1}	V, km s^{-1}	W, km s^{-1}	$R_{\rm min}$, kpc	$R_{\rm max}$, kpc	$Z_{\rm max}$, kpc	e
1	2901	24.4 ± 13.0	-144.5 ± 9.1	-36.9 ± 8.9	2.17 ± 0.16	8.67 ± 0.03	0.42 ± 0.10	0.60 ± 0.02
2	10550	-57.5 ± 3.4	-42.1 ± 2.7	3.0 ± 2.2	6.11 ± 0.07	9.97 ± 0.07	0.36 ± 0.00	0.24 ± 0.01
3	92095	67.6 ± 2.3	-54.2 ± 3.2	22.1 ± 0.6	5.62 ± 0.08	9.42 ± 0.04	0.46 ± 0.01	0.25 ± 0.01
4	94600	20.5 ± 0.6	-18.3 ± 0.4	-36.9 ± 0.4	8.17 ± 0.01	8.74 ± 0.01	0.41 ± 0.00	0.03 ± 0.00
5	94669	-41.7 ± 0.7	-43.3 ± 1.6	-38.2 ± 0.5	6.19 ± 0.04	9.39 ± 0.02	0.45 ± 0.00	0.21 ± 0.00
6	94860	20.4 ± 2.5	-59.9 ± 1.5	-43.9 ± 0.7	5.73 ± 0.04	8.62 ± 0.01	0.55 ± 0.01	0.20 ± 0.01
7	99902	-3.3 ± 0.3	-23.8 ± 2.0	-39.3 ± 0.8	7.77 ± 0.06	8.75 ± 0.02	0.47 ± 0.01	0.06 ± 0.00
8	100696	-40.7 ± 0.6	-20.4 ± 0.3	35.8 ± 0.6	7.24 ± 0.01	10.01 ± 0.02	0.76 ± 0.01	0.16 ± 0.00
9	104985	-76.2 ± 1.6	-8.5 ± 0.3	30.5 ± 1.1	6.91 ± 0.02	12.15 ± 0.04	0.74 ± 0.02	0.28 ± 0.00
10	127243	78.6 ± 2.0	-111.0 ± 2.7	53.0 ± 1.5	3.30 ± 0.05	9.15 ± 0.02	1.21 ± 0.03	0.47 ± 0.01
11	141353	-8.9 ± 3.3	-69.9 ± 4.1	-56.3 ± 1.3	5.17 ± 0.11	8.47 ± 0.01	0.81 ± 0.02	0.24 ± 0.01
12	141472	155.0 ± 11.7	-71.2 ± 5.1	63.7 ± 5.1	4.10 ± 0.10	12.74 ± 0.37	1.96 ± 0.13	0.51 ± 0.02
13	152879	10.1 ± 0.8	-28.5 ± 1.6	58.3 ± 2.4	7.87 ± 0.06	8.41 ± 0.00	1.22 ± 0.04	0.03 ± 0.00
14	197752	-78.1 ± 3.2	-6.6 ± 1.6	-44.7 ± 1.8	6.88 ± 0.04	12.23 ± 0.10	0.67 ± 0.02	0.28 ± 0.01

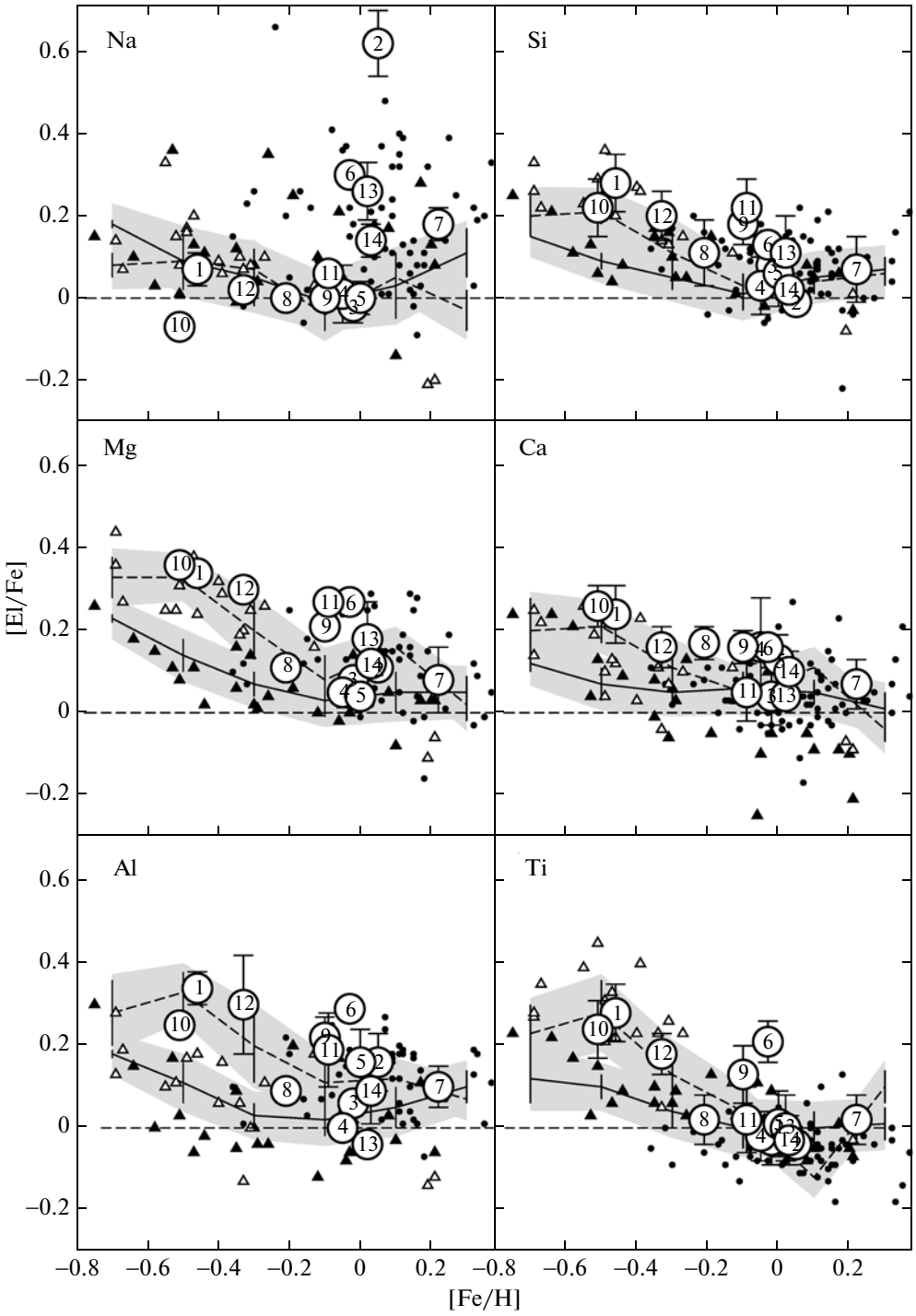

Fig. 2. [Na, Mg, Al, Si, Ca, Ti/Fe] abundance trends with metallicity in the atmospheres of the red giants investigated here (the large circles with the star numbers from Table 1) in comparison with the thin-disk red giants that we studied previously (filled small circles), the thin- and thick-disk red giants from Alves-Brito et al. (2010) (filled and open triangles), and the thin- and thick-disk dwarfs from Bensby et al. (2005) (the solid and dashed lines in the shaded regions).

Figure 3 presents the s-element [Y/Fe] and [Ba/Fe] and r-element [Eu/Fe] abundance trends with metallicity. The designations in the figure are similar to those in Fig. 2. This figure does not present all stars. For example, the Y II lines in some cases are too weak for their equivalent widths to be properly measured, while the Ba II lines, on the contrary, often have an equivalent width larger than 100–150 mÅ.

In this case, the line wings and the significantly growing influence of non-LTE processes play a great role. All of this makes it impossible to determine the barium abundance in this technique with an accuracy characteristic of other elements (about 0.1 dex).

Sodium

The sodium abundance was determined from the Na I 6154 and 6160 Å lines without any correction for non-LTE processes. According to Korotin and Komarov (1989), Mashonkina et al. (2000), and Lind et al. (2011), this doublet is formed deeper than other sodium lines, and the non-LTE processes do not introduce significant corrections to the abundance determination. We see from Fig. 2 that a substantial fraction of the program stars are located above the dwarfs that lie compactly (the shaded region). Such a behavior is also typical of the previously studied red giants and the thin-disk giants from Alves-Brito et al. (2010) and suggests that the [Na/Fe] abundance is determined not only by the chemical evolution of the Galaxy but also by the evolution of the star itself.

The observed sodium overabundances in the atmospheres of red giants were pointed out back in 1963 (G. Cayrel and R. Cayrel 1963). When investigating the chemical composition of the red giant ϵ Vir, the authors found that the abundances of most elements were solar, within the error limits, while sodium was slightly overabundant. Helfer and Wallerstein (1964) also described the observed overabundances in the atmospheres of red giants in the Hyades open clyster. When investigating the chemical composition of red giants, the same authors (Helfer and Wallerstein 1968) found several stars with an enhanced [Na/Fe] abundance and pointed out a systematic difference in sodium abundance between red giants and dwarfs. When the results were discussed, it was hypothesized that sodium is synthesized in some red giants. In 1970, Cayrel de Strobel et al. (1970) ascertained that the [Na/Fe] abundance increases with temperature parameter $\theta = 5040/T_{\rm eff}$.

The observed sodium overabundances in the atmospheres of supergiants were detected in 1981 (A. Boyarchuk and M. Boyarchuk 1981; Boyarchuk and Lyubimkov 1981). It was then also shown that the overabundance depends on surface gravity $\log g$ or luminosity. Subsequently, these authors hypothesized that sodium could be produced in the ^{22}Ne(p,γ)^{23}Na reaction that enters the neon–sodium cycle of hydrogen burning in the cores of main-sequence stars and could then be brought from deep layers into the stellar atmosphere through developing convection as the star evolves from the main sequence to the red giant branch (Boyarchuk and Lyubimkov 1983). The calculations performed by Denisenkov and Ivanov (1987) and Denisenkov (1988) confirmed that this hypothesis is possible. Subsequent calculations using new nuclear reaction

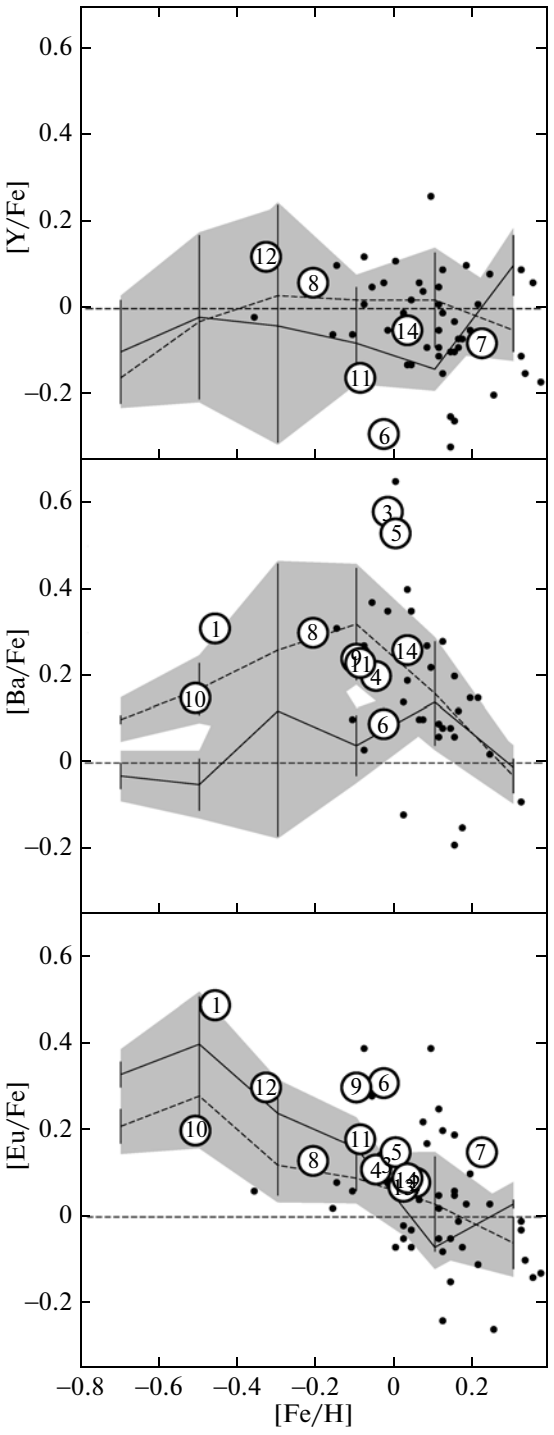

Fig. 3. [Y, Ba, Eu/Fe] abundance trends with metallicity in the atmospheres of the investigated red giants in comparison with the data for other stars. The notation is the same as that in Fig. 2.

characteristics also showed a change of the sodium abundance in red giants (Cavallo et al. 1996, 1998). Although the neon–sodium cycle requires high temperatures and is efficient only in massive stars, low-mass ($1-3M_\odot$) stars can also produce sodium.

The stable isotope ^{23}Na is currently believed to be produced mainly in the carbon burning reaction $^{12}C(^{12}C,p)^{23}Na$. A small amount can also be produced in the hydrogen, $^{22}Ne(p,\gamma)^{23}Na$, and helium, $^{14}N(\alpha,\gamma)^{19}F(\alpha,\gamma)^{23}Na$, burning reactions (Woosley and Weaver 1995). The first and last reactions do not proceed in red giants at the shell hydrogen burning stage, but the second reaction is possible. Thus, the helium and carbon burning reactions in stars of earlier generations for red giants determine some basic sodium abundance, as in the case of dwarfs, and the amount of sodium produced in the stellar interior over its lifetime on the main sequence in the hydrogen burning reaction is added to this value. According to the calculations published in the review by Wallerstein et al. (1997), the ^{23}Na abundance at a temperature $T = 0.05 \times 10^9$ K and a pressure of 100 g cm^{-3} in the stellar core increases by a factor of 7 in 100 yr. However, there are large uncertainties in the data on the $^{22}Ne(p,\gamma)^{23}Na$ reaction cross sections and rates under conditions of low temperatures in the stellar cores.

Subsequently, it was shown that the observed [Na/Fe] overabundances in the atmospheres of normal red giants also depend on surface gravity (Boyarchuk et al. 2001), with this dependence being an extension of the dependence for supergiants noted above. Interestingly, [Na/Fe] overabundances were also detected in the atmospheres of various classes of red giants: moderate and classical barium stars (Boyarchuk et al. 2002; Antipova et al. 2004), supermetal-rich stars (Pakhomov et al. 2009a, 2009b), whose positions satisfy the same dependence as that for the remaining normal red giants. The subsequent sodium abundance analyses for the atmospheres of red giants performed at the Institute of Astronomy, the Russian Academy of Sciences, showed that some stars have a reduced [Na/Fe] abundance relative to the observed dependence on surface gravity (Antipova et al. 2005; Pakhomov et al. 2009a, 2009b). The kinematic characteristics of such stars correspond to thick-disk objects.

In Fig. 2, HD 10550 lies above the remaining stars and has a sodium abundance that is higher than that for dwarfs at the same metallicity approximately by 0.5 dex. Among all of our program stars, HD 10550 has the lowest surface gravity $\log g = 1.25$. HD 152879 also lies statistically above the dwarfs ($\log g = 1.80$). The remaining stars lie, within the error limits, in the region where the dwarfs are located, except HD 127243; it has a [Na/Fe] abundance that is lower than that for dwarfs approximately by 0.15 dex.

In Fig. 4, the [Na/Fe] abundance is plotted against the surface gravity $\log g$ in the atmospheres of the program stars in comparison with the previously studied thin- and thick-disk red giants. We see that the positions of the thin-disk stars form a distinct dependence, while the thick-disk stars with a reduced [Na/Fe] abundance lie below it. In this figure, most of the program stars are also located below the dependence for the thin-disk giants in the region where the thick-disk stars dominate. For some of the stars with a relatively low metallicity (HD 127243 [Fe/H] $= -0.44$ and HD 141472 [Fe/H] $= -0.27$), the [Na/Fe] underabundance reaches 0.5 dex. The stars from Table 1 with a high probability of their membership in the thin disk but with a large orbital parameter $Z_{\max}$ (HD 94600, HD 99902, and HD 100696) are located at the lower boundary of the region for the thin-disk giants and at its upper boundary for the thick-disk giants. In this case, we cannot determine with confidence which dynamical subsystem of the Galaxy they belong to from Fig. 4.

The causes of the reduced sodium abundance in the atmospheres of thick-disk red giants relative to the [Na/Fe]–$\log g$ relation can be: (1) the initial sodium underabundance; (2) the initial neon underabundance that led to the production of a smaller amount of sodium; and (3) the shallower convective shell. The first assumption is not backed by the observational data; the [Na/Fe] abundances in the thick- and thin-disk dwarfs differ only slightly. The second assumption can possibly play a significant role, but it is difficult to test this hypothesis at present due to the absence of accurate data on the neon abundances in thick-disk stars. The last assumption is unlikely, because the physical parameters of the stars ($T_{\rm eff}$, $\log g$, [Fe/H], mass) with normal and reduced [Na/Fe] abundances are identical and it would be unreasonable to expect the convective processes in them to differ noticeably.

Among the program thick-disk stars, there are two with a significant [Na/Fe] abundance relative to other stars with similar parameters. The first star HD 94860 is located in a region characteristic of the metal-rick thin-disk stars. For example, the Hyades giants (with [Fe/H] ≈ 0.14 dex) are also located there. The equivalent widths of the sodium 6154 and 6160 Å lines are 85 and 105 mÅ, respectively; such very close values were also measured for HD 94669 with similar $\log g$ and [Fe/H], but this star has a much lower temperature (by 250 K) and, hence,

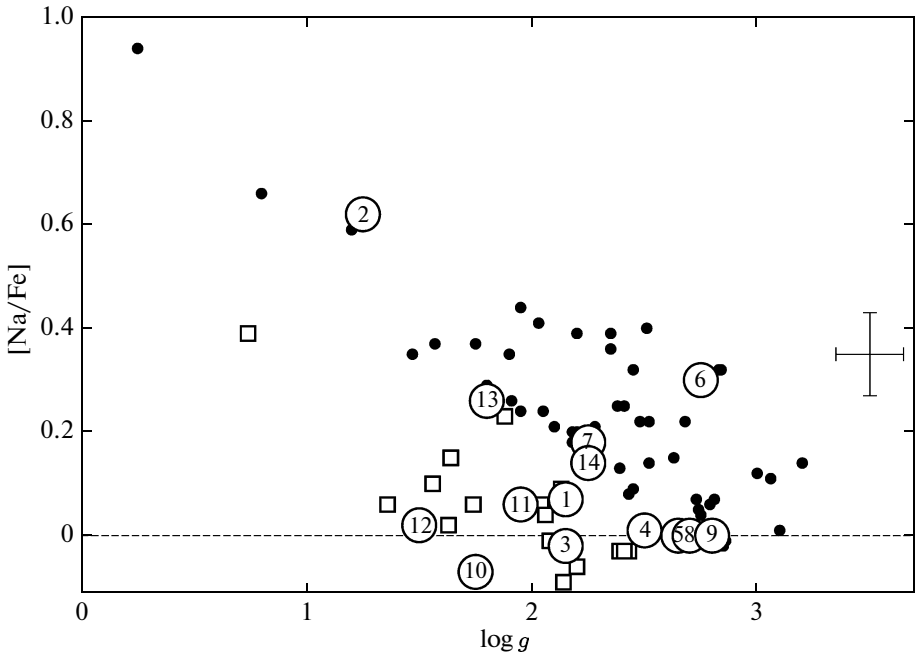

Fig. 4. [Na/Fe] abundance versus surface gravity $\log g$ in the atmospheres of our red giants (large open circles) and the previously investigated thin-disk (filled circles) and thick-disk (open squares) red giants. The possible error bars are indicated on the right.

a low abundance [Na/Fe] = 0.00 dex. Since the errors in the [Na/Fe] abundance (see Table 4) cannot change it greatly, the estimated sodium abundance in HD 94860 is realistic. This star, which kinematically belongs to the thick disk, may have been formed in a gas–dust cloud similar in chemical composition to the thin-disk objects. The second star HD 10500 is located in Fig. 4 near the thin-disk supergiants. However, it has the highest mass among the program stars ($7M_{\odot}$) and, consequently, the internal physical conditions under which sodium is synthesized more efficiently. The star may also have a deeper convective envelope that provides the rise of sodium from the stellar interior.

Magnesium

In Fig. 2, all of the program stars are located, within the magnesium abundance error limits, in the region of dwarfs. Three red giants with the lowest iron abundance (HD 127243, HD 2901, and HD 141472) clearly correspond to the distribution of thick-disk stars. In this region with [Fe/H] $\lesssim -0.3$, the separation of the thin- and thick-disk dwarfs is largest (about 0.2 dex) and exceeds the mean abundance errors (about 0.1 dex). The data on the giants from Alves-Brito et al. (2010) also closely correspond to the trends for the dwarfs: the thin-disk giants lie along the solid line, while the thick-disk giants lie along the dashed line.

Magnesium is produced in the carbon, $^{16}\mathrm{O}(^{12}\mathrm{C},\ \alpha)^{24}\mathrm{Mg}$, helium, $^{20}\mathrm{Ne}(\alpha,\gamma)^{24}\mathrm{Mg}$, $^{21}\mathrm{Ne}(\alpha,n)^{24}\mathrm{Mg}$, and hydrogen, $^{23}\mathrm{Na}(p,\gamma)^{24}\mathrm{Mg}$, $^{27}\mathrm{Al}(p,\alpha)^{24}\mathrm{Mg}$, burning reactions. The case of carbon and helium burning plays no role in the chemical evolution during the lifetime of red giants, while the last hydrogen burning reaction in the magnesium–aluminum cycle is mots likely inefficient, because this requires conditions with much higher temperatures than those in low-mass stars at the red giant stage. Only the reaction with sodium involvement $^{23}\mathrm{Na}(p,\gamma)^{24}\mathrm{Mg}$ can slightly raise the magnesium abundance (Wallerstein et al. 1997). This may underlie the slight [Mg/Fe] overabundance for some normal red giants. However, the entire effect is within the 2σ magnesium abundance error limits.

Aluminum

In Fig. 2, all of the program stars are located, within the aluminum abundance error limits, in the region of dwarfs. Just as in the case of magnesium, three red giants with the lowest iron abundance (HD 127243, HD 2901, and HD 141472) clearly correspond to the distribution of thick-disk dwarfs. The data from Alves-Brito et al. (2010) show a larger

scatter of abundances relative to the dwarfs than that for magnesium. Some of the previously studied red giants are located approximately 0.2 dex higher than the dwarfs. Although this difference does not exceed the 2σ level, the published data suggest an enhanced aluminum abundance in globular cluster giants (Cavallo et al. 1996).

In stars, aluminum can be produced in two reactions of the magnesium–aluminum cycle of hydrogen burning: $^{26}\mathrm{Mg}(p,\gamma)^{27}\mathrm{Al}$ and $^{26}\mathrm{Al}(p,\gamma)^{27}\mathrm{Si}(\beta^{+}\nu_e)^{27}\mathrm{Al}$. The physical parameters needed for the ^{27}Al production reaction were estimated by Fujimoto et al. (1999), who described the possibility of the existence of observable aluminum overabundances in the atmospheres of red giants.

Silicon

In Fig. 2, all of the program stars are located within the silicon abundance error limits, in the region of dwarfs. Just as in the case of magnesium and aluminum, three red giants with the lowest iron abundance (HD 127243, HD 2901, and HD 141472) correspond to the distribution of thick-disk dwarfs.

The isotope ^{28}Si is produced mainly in the oxygen burning reaction $^{16}\mathrm{O}(^{16}\mathrm{O},\alpha)^{28}\mathrm{Si}$, which is inaccessible for low-mass red giants. The $^{27}\mathrm{Al}(p,\gamma)^{28}\mathrm{Si}$ reaction entering the magnesium–aluminum cycle of hydrogen burning can be a possible silicon production source, but its contribution to nucleosynthesis in low-mass stars is negligible and is considered as a leakage reaction (Cavallo et al. 1996).

Calcium

In Fig. 2, almost all of the program stars are located, within the calcium abundance error limits, in the region of dwarfs. Just as in the case of magnesium and aluminum, three red giants with the lowest iron abundance (HD 127243, HD 2901, and HD 141472) correspond to the distribution of thick-disk dwarfs.

Calcium is an α-element and it originates in the oxygen burning reactions. The calcium abundance does not change over the lifetime of a red giant.

Titanium

Titanium, along with magnesium, silicon, and calcium, is an α-element and, at the same time, also belongs to the iron-peak elements produced during supernova 1a explosions. Just as other α-elements, titan is characterized by an increase in its abundance with decreasing metallicity. Just as in the case of magnesium, aluminum, silicon, and calcium, three red giants with the lowest iron abundance (HD 127243, HD 2901, and HD 141472) correspond to the distribution of thick-disk dwarfs. A slightly overestimated titanium abundance was determined for HD 94860, but it is within the 1σ error limits relative to the dwarfs.

Yttrium

As one of the s-elements, yttrium is produced in the slow neutron capture process. The presence of a flux of free neutrons is necessary for this process. This condition is met in stars at the asymptotic giant branch stage—a later evolutionary stage relative to the normal red giants. Therefore, the same picture as that for the dwarf stars must be observed (Fig. 3).

However, this figure does not present the moderate and classical barium stars investigated previously (Boyarchuk et al. 2002; Antipova et al. 2004). In classical barium stars, binarity plays a major role—one of the binary components evolves more rapidly and ejects its envelope rich in s-elements part of which is captured by the secondary component. They are characterized by a different, steeper trend with decreasing metallicity (Antipova et al. 2004). In contrast, for moderate barium stars, some of which can be represented by single red giants, possible photoneutron reactions like $^{13}\mathrm{C}(\gamma,n)^{12}\mathrm{C}$ and $^{14}\mathrm{N}(\gamma,n)^{13}\mathrm{N}$ can play a role. According to Harrison and Edwards (1974), when the CNO cycle of hydrogen burning proceeds in the interior of a main-sequence star, a large number of energetic gamma-ray photons capable of knocking out a neutron from the nuclei of some elements emerge. This source of neutrons is weak, but, as was pointed out by Harrison and Edwards (1974), it is the second in intensity among all of the known neutron sources and could possibly explain the small anomalies of s-process elements observed in stars at the red giant stage.

Barium

In Fig. 3, all of the program stars, except two, lie in the region of dwarfs. These stars (HD 92095 and HD 94669) have the most saturated barium lines among the stars presented on the plot and probably the largest errors in the barium abundance. The most metal-poor stars HD 127243 and HD 2901 are located in a region characteristic of the thick-disk dwarfs.

Europium

Europium is an r-element whose origin is associated with the rapid neutron capture process that occurs during supernova explosions, and its abundance does not change during the evolution of a red

giant. Within the error limits, the program stars are located in the same region as the dwarfs and exhibit an increase in [Eu/Fe] abundance with decreasing metallicity.

CONCLUSIONS

We investigated 14 red giants with high space velocities. For all stars, we determined their Galactic orbital elements and other kinematic characteristics from which their membership in a particular Galactic subsystem can be judged. We determined the physical parameters, stellar atmosphere parameters, and elemental abundances. For almost all chemical elements, their abundance trends with metallicity were shown to correspond to those for dwarfs. Where a significant difference exists between the trends corresponding to the thin- and thick-disk dwarfs, the positions of the thick-disk giants follow the trend for the thick-disk dwarfs. An abundance analysis of the atmospheres of red giants provides an additional possibility to determine whether a star belongs to the Galactic thick or thin disk in some cases. A different picture is observed for sodium: in addition to the dependence on metallicity, which is determined by the chemical evolution of the Galaxy, there is a significant dependence on surface gravity $\log g$, which reflects the degree of development of the convective envelope in a red giant. In this case, there is a significant difference between the [Na/Fe] abundances in the atmospheres of thick- and thin-disk red giants.

ACKNOWLEDGMENTS

This work was supported by the Russian Foundation for Basic Research (project nos. 09-02-00528-a, 12-02-00610-a), the "Origin, Structure, and Evolution of Objects in the Universe" Program of the Presidium of the Russian Academy of Sciences, and the Federal Agency for Science and Innovations (State contract no. 02.740.11.0247).

REFERENCES

1. C. Allen and A. Santillan, Rev. Mex. Astron. Astrofis. **22**, 255 (1991).
2. A. Alves-Brito, J. Meléndez, M. Asplund, et al., Astron. Astrophys. **513**, A35 (2010).
3. L. I. Antipova and A. A. Boyarchuk, Astron. Rep. **45**, 700 (2001).
4. L. I. Antipova, A. A. Boyarchuk, Yu. V. Pakhomov, et al., Astron. Rep. **47**, 648 (2003).
5. L. I. Antipova, A. A. Boyarchuk, Yu. V. Pakhomov, et al., Astron. Rep. **48**, 597 (2004).
6. L. I. Antipova, A. A. Boyarchuk, Yu. V. Pakhomov, et al., Astron. Rep. **49**, 535 (2005).
7. T. Bensby, S. Feltzing, I. Lundström, et al., Astron. Astrophys. **433**, 185 (2005).
8. M. S. Bessell, F. Castelli, and B. Plez, Astron. Astrophys. **333**, 231 (1998).
9. A. A. Boyarchuk and M. E. Boyarchuk, Izv. KRAO **63**, 68 (1981).
10. A. A. Boyarchuk, L. I. Antipova, M. E. Boyarchuk, et al., Astron. Rep. **45**, 301 (2001).
11. A. A. Boyarchuk, L. I. Antipova, Yu. V. Pakhomov, et al., Astron. Rep. **46**, 819 (2002).
12. A. A. Boyarchuk, L. I. Antipova, Yu. V. Pakhomov, Astron. Rep. **52**, 630 (2008).
13. A. A. Boyarchuk and L. S. Lyubimkov, Izv. KRAO **64**, 1 (1981).
14. A. A. Boyarchuk and L. S. Lyubimkov, Izv. KrAO **66**, 130 (1983).
15. F. Castelli and R. L. Kurucz, in *New Grids of ATLAS9 Model Atmospheres, Proceedings of the IAU Symposium No. 210,* Ed. by N. E. Piskunov, W. W. Weiss, and D. F. Gray (ASP, San Francisco, 2003), Vol. 210, p. 20.
16. R. M. Cavallo, A. V. Sweigart, and R. A. Bell, Astrophys. J. **464**, L79 (1996).
17. R. M. Cavallo, A. V. Sweigart, and R. A. Bell, Astrophys. J. **492**, 575 (1998).
18. G. Cayrel and R. Cayrel, Astrophys. J. **137**, 431 (1963).
19. G. Cayrel de Strobel, J. Chauve-Godard, G. Hernandez, et al., Astron. Astrophys. **7**, 408 (1970).
20. B. Chen, C. Stoughton, J. A. Smith, et al., Astrophys. J. **553**, 184 (2001).
21. P. A. Denisenkov, Sov. Astron. Lett. **14**, 435 (1988).
22. P. A. Denisenkov and V. V. Ivanov, Sov. Astron. Lett. **13**, 214 (1987).
23. O. J. Eggen, Mon. Not. R. Astron. Soc. **118**, 65 (1958a).
24. O. J. Eggen, Mon. Not. R. Astron. Soc. **118**, 154 (1958b).
25. B. Famaey, A. Jorissen, X. Luri, et al., Astron. Astrophys. **430**, 165 (2005).
26. M. Y. Fujimoto, M. Aikawa, and K. Kato, Astrophys. J. **519**, 733 (1999).
27. G. Gilmore and N. Reid, Mon. Not. R. Astron. Soc. **202**, 1025 (1983).
28. L. Girardi, A. Bressan, G. Bertelli, et al., Astron. Astrophys. Suppl. Ser. **141**, 371 (2000).
29. T. G. Harrison and T. W. Edwards, Astrophys. J. **187**, 303 (1974).
30. H. L. Helfer and G. Wallerstein, Astrophys. J. Suppl. Ser. **9**, 81 (1964).
31. H. L. Helfer and G. Wallerstein, Astrophys. J. Suppl. Ser. **16**, 1 (1968).
32. S. A. Korotin and N. S. Komarov, Sov. Astron. **33**, 449 (1989).
33. R. Kurucz, *ATLAS9 Stellar Atmosphere Programs and 2 km/s Grid. Kurucz CD-ROM No. 13.* (Cambridge, Mass.: Smithsonian Astrophys. Observ., 1993), Vol. 13.
34. V. A. Kutvitskii, V. B. Semikoz, and D. D. Sokolov, Astron. Rep. **53**, 166 (2009), arXiv: 0809.3172.

35. F. van Leeuwen, Astron. Astrophys. **474**, 653 (2007).
36. K. Lind, M. Asplund, P. S. Barklem, et al., Astron. Astrophys. **528**, A103 (2011).
37. L. I. Mashonkina, V. V. Shimanskii, and N. A. Sakhibullin, Astron. Rep. **44**, 790 (2000).
38. E. Maurice, J. Andersen, A. Ardeberg, et al., Astron. Astrophys. Suppl. Ser. **67**, 423 (1987).
39. T. V. Mishenina, C. Soubiran, V. V. Kovtyukh, et al., Astron. Astrophys. **418**, 551 (2004).
40. Yu. V. Pakhomov, L. I. Antipova, A. A. Boyarchuk, et al., Astron. Rep. **53**, 660 (2009a).
41. Yu. V. Pakhomov, L. I. Antipova, A. A. Boyarchuk, et al., Astron. Rep. **53**, 685 (2009b).
42. Yu. V. Pakhomov, L. I. Antipova, and A. A. Boyarchuk, Astron. Rep. **55**, 256 (2011).
43. A. C. Robin, M. Haywood, M. Creze, et al., Astron. Astrophys. **305**, 125 (1996).
44. G. Wallerstein, I. Iben, P. Parker, et al., Rev. Mod. Phys. **69**, 995 (1997).
45. S. E. Woosley and T. A. Weaver, Astrophys. J. Suppl. Ser. **101**, 181 (1995).

Translated by V. Astakhov